A Geodetic-Based Earthquake Early Warning System for Colombia and Ecuador

Lusette Karime Escobar-Rey[1], David Mencin[*2], Tim Dittmann[2], Patricia A. Mothes[3], and Héctor Mora-Páez[1]

Abstract

Colombia and Ecuador sit at one of the most diverse tectonic regimes in the world, located at the intersection of five tectonic plates (Bird, 2003) encompassing many geophysical hazard regimes, multiple subduction zones, and broad diffuse areas of significant deformation. Notably, the subduction of the Nazca plate under South America has produced at least seven large ($> M_w$ 7) and damaging earthquakes since 1900—the largest being the 1906 M_w 8.8 event. Both Colombia and Ecuador have made significant investments in Global Navigation Satellite System (GNSS) networks to study tectonic and volcanic deformation. Earthquake early warning (EEW) systems like the U.S.-operated ShakeAlert system (Murray *et al.*, 2018, 2023) utilize real-time Global Navigation Satellite System (RT-GNSS) to rapidly characterize the largest, most damaging earthquakes in situations where seismic networks alone saturate (Melgar *et al.*, 2015, 2016; Allen and Melgar, 2019; Ruhl *et al.*, 2019). Both Colombia and Ecuador have large vulnerable populations proximal to the coast that may sustain significant damage in these large subduction events (Pulido *et al.*, 2020) and yet farther enough away that an RT-GNSS EEW system could offer significant warning times to these populations and associated infrastructure. We examine the status of the Servicio Geológico Colombiano Geodesia: Red de Estudios de Deformación GNSS network in Colombia and the Escuela Politécnica Nacional GNSS network in Ecuador, their spatial distribution, and the current status of their data streams to determine what augmentations are required to support the real-time detection and modeling of large destructive earthquakes in and near Colombia and Ecuador.

Cite this article as Escobar-Rey, L. K., D. Mencin, T. Dittmann, P. A. Mothes, and H. Mora-Páez (2024). A Geodetic-Based Earthquake Early Warning System for Colombia and Ecuador, *Seismol. Res. Lett.* **96**, 294–309, doi: 10.1785/0220230390.

Description of Geologic Setting, Network History, and Current Status

Colombia and Ecuador sit at one of the most diverse tectonic regimes in the world, located at the intersection of five tectonic plates (Bird, 2003) (Caribbean, Panama block, North Andes block, Nazca, and South America) encompassing many geophysical hazard regimes, multiple subduction zones, and broad diffuse areas of significant deformation (Mora-Páez *et al.*, 2018). In particular, the subduction of the Nazca plate under South America has produced at least seven large (M_w 7+) and damaging earthquakes since 1900—the largest being the 1906 M_w 8.8 event (Pulido *et al.*, 2020). This northwest corner of South America is marked by a broad area of deformation of nearly 1,000,000 sq. km, accommodating the relative motions of the Nazca, Cocos, Caribbean, and South American plates along with numerous blocks. The western extent of this region below ~5° N, marked by the subduction of the Nazca plate under South American and the Cocos plates under the Central American isthmus, produces relatively frequent major earthquakes. The region is roughly defined from 5° N northward to the Caribbean and from the West Coast of South America, through the Panama Isthmus, to the Maracaibo basin. It is marked by the broad diffuse seismicity and yet unknown hazards. Although this study focuses primarily on the better-constrained events occurring along the subduction of the Nazca plate under Colombia's Pacific coast; other well-established areas of seismogenic hazard exist throughout the country. Colombia has a diverse set of additional seismogenic zones capable of generating large destructive earthquakes, including subduction under the Caribbean coast (Bilham and Mencin, 2013; Mencin, 2018; Lizarazo *et al.*, 2021) and significant strike-slip fault systems throughout the country (Taboada *et al.*, 2000; Velandia *et al.*, 2005; Acosta *et al.*, 2007).

1. Servicio Geologico Colombiano, Bogotá, Colombia, https://orcid.org/0000-0002-6769-6482 (LKE-R); 2. EarthScope Consortium, Washington DC, U.S.A., https://orcid.org/0000-0001-9984-6724 (DM); https://orcid.org/0000-0002-6104-7190 (TD); 3. Instituto Geofísico, Escuela Politécnica Nacional, Quito-Ecuador, Quito, Ecuador

*Corresponding author: david.mencin@earthscope.org

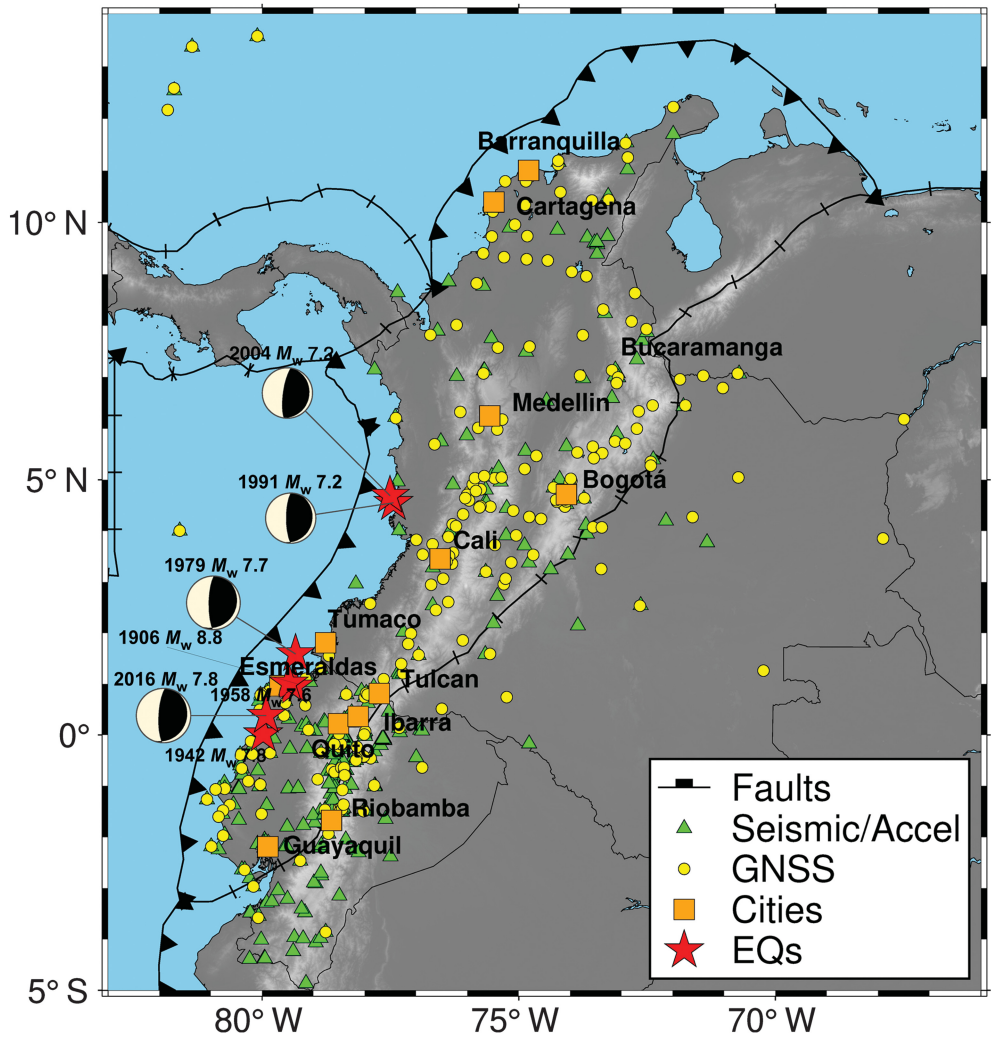

Figure 1. Existing Global Navigation Satellite System (GNSS) and Seismic Networks. The green triangles are the existing seismic or strong-motion stations, yellow dots are currently installed GNSS stations (most of these are not, at present, real-time), red stars are the seven historical earthquakes used in this study from Pulido *et al.* (2020), and orange squares are the twelve metro areas considered in this study.

Both Colombia and Ecuador have made significant investments in Global Navigation Satellite System (GNSS) networks to study tectonic and volcanic deformation. In Colombia, space-based geodesy began in 1988 with the Central and South America (CASA) Global Positioning System (GPS) project, involving 25 organizations from 13 countries, creating one of the first GPS satellite-tracking networks to study plate tectonics (Freymueller *et al.*, 1993; Trenkamp *et al.*, 2002). To further constrain the geodynamics of northwestern South America, the Servicio Geológico Colombiano established the Geodesia: Red de Estudios de Deformación (GeoRED) network beginning in 2007 building on the previous effort of the CASA project. Today the Colombian GNSS network, mostly composed of GeoRED, is composed of 228 continuous stations that span the length and width of Colombia (Fig. 1). The GeoRED network in Colombia is composed of Trimble receivers, mainly R9 and Alloy models, along with choke-ring and Zephyr-2 antennas. The data transmission is based on satellite internet, local networks of institutions where the stations are located, and in some cases, by cellular modem. ~20 of these stations currently provide real-time data, and a total of about ~100 could easily be upgraded to real-time; the remaining stations would require upgrades to power systems and/or communication systems. Ecuador, also involved in the CASA project with ~90 campaign-style GPS sites, established the National Geodetic Network (RENGEO) in 2006, initially focused on areas with greater volcanic activity. In 2008, it was expanded into a regional network today composed of 80 continuous GNSS stations countrywide with a focus on the tectonically active regions (Alvarado *et al.*, 2018). The RENGEO network is mostly composed of Trimble receivers: Trimble NetRS, NetR9, and Alloy; with three stations operating a Leica GR50. Antenna types are Trimble Zephyr Geodetic 1, 2, and 3 and three Leica AS11 antennas. Communication varies between microwave, satellite, radio, and cellular modem. Currently, ~10 stations operate in real-time.

Methods

Beginning in the early 2000s, many countries around the world began developing EEW and tsunami warning systems based on already existing seismic networks. These systems rely on the rapid detection of earthquakes based on seismometers using *P*-wave arrival times and then transmitting information about the earthquake determined both by seismometers, and, recently, GNSS to locations further afield before the arrival of the destructive *S* wave, providing seconds to minutes of warning to mitigate damage to infrastructure and even give citizens time to react and take precautionary measures (Crowell *et al.*, 2013; Allen and Melgar, 2019; Ruhl *et al.*, 2019). Large earthquakes (M_w 7+),

those with the most damage potential, presented technical issues in that seismic instruments saturate, leaving the seismic system blind until the seismic waves have traveled farther enough away that they did not saturate the instruments. Warnings in these cases come after the destructive energy has passed. GNSS proved to be a suitable tool for EEW applications for large earthquakes and was adopted by many countries as a critical addition to EEW operations. An excellent and more complete description of EEW exists here (Ruhl *et al.*, 2017, 2019; Allen and Melgar, 2019).

In this study, we posit the use of GNSS networks for both detection and magnitude determination because the seismic network in Colombia is sparse and would create large shadow zones resulting in delays in warning times that are unacceptable. Although this limits the capabilities of the network in detecting and issuing warnings for smaller earthquakes, an essential aspect of the human acceptance and reaction to these warnings, the GNSS networks are already in place and with minimal relative investment can be made operational. The relative trade-offs are addressed in Grapenthin *et al.* (2017).

Most, if not all, existing EEW systems rely on broadband seismic instruments to detect and locate the earthquake using the *P* wave, before reaching saturation, during large events. This seeding or initialization allows one to rapidly determine both where and when an event happened. In the case of large earthquakes (M_w >6.5), GNSS is then used to determine the magnitude based on empirical relationships (Crowell *et al.*, 2013; Melgar *et al.*, 2015; Murray *et al.*, 2023). These hybrid systems optimize relative input sensor strengths to allow for the detection and accurate characterization of a large range of earthquake magnitudes. This study evaluates EEW for the largest, most destructive events based only on GNSS instruments because of the lack of available broadband and strong-motion instruments in the region. Furthermore, even an optimized hybrid EEW system that can operate with inputs from different sensors independently will inherently be more robust in the case of sensor or network failures. Although beyond the scope of this article, we address the issue of seeding or initializing the inversion without inertial sensors with three plausible detection methods:

1. Crowell *et al.* (2009) proposed using a method of strain triangulation, where an earthquake was detected when a strain threshold was exceeded in any given triangle constructed with the installed GNSS receivers. We do not believe this will perform well in this scenario because the strain triangles are large and introduce large uncertainties, and the most destructive examples used lie offshore and beyond the abilities of this method.
2. More promising is the recent work with machine learning aimed at differentiating coseismic ground motion in GNSS signals both in peak ground displacement (PGD) space and phase observable space directly along with the precise timing that can be used for triangulation (Dittmann, Hodgkinson, *et al.*, 2022; Dittmann, Liu, *et al.*, 2022).
3. Finally, a more direct approach would be to use the data assimilation directly as large amplitude deviations are detected spatially, as laid out in Hossen *et al.* (2021).

A second aspect to address is the use of point sources when calculating the warning times. In the United States, the EEW system currently operational is called ShakeAlert and is operated by the U.S. Geological Survey (USGS) (Given, 2014, 2018). ShakeAlert uses three different algorithms to determine the earthquake location, origin time, and magnitude: the Earthquake Point-source Integrated Code (EPIC), which uses *P* waves measured with seismometers to estimate the location and origin time when assuming a fixed depth of 8 km and a point source. It then calculates magnitude using an empirical scaling relationship between source–station distance and the peak displacement of the *P* wave (Chung *et al.*, 2019), the finite-fault rupture detector (FinDer) that matches observed acceleration to precomputed templates to identify the location, orientation, and length of a line source and then infers magnitude from the length-scaling relationships (Böse *et al.*, 2017) and geodetic first approximation of size and timing (GFAST)-PGD, which is seeded with the seismically derived location and assumes a point source and then uses PGD from real-time Global Navigation Satellite System (RT-GNSS) and empirically derives a magnitude (Crowell *et al.*, 2018; Murray *et al.*, 2023). These solutions are then fed into a solution aggregator to determine the final magnitude for the issued warning; the aggregator favors GFAST-PGD above M_w 6.5 (Murray *et al.*, 2023). It has been shown that in current EEW systems, especially those that use FinDer, there is an inherent sensitivity to the use of point sources. In fact, FinDer now utilizes a "line" source to overcome this sensitivity. These sensitivities are driven by the high-frequency noise in the broadband zero-baseline part of the system. Even with this shortcoming addressed by using line sources, FinDer itself now uses RT-GNSS for large earthquakes using point sources significantly improving its performance for large earthquakes. In addition, EPIC also uses point sources for their magnitude detection without the sensitivities in the FinDer pattern-matching approach. Given that GNSS inversions for magnitude use point sources, we use point sources in our warning time simulations. We acknowledge a possible drawback in the use of point sources when making these simulations that times may be misleading if the point source is placed at the hypocenter. Given that some of these historic earthquakes lack hypocenter information but have approximate centroid information, we use the best available data in the simulation. A possible alternate and more conservative approach would be to use whichever is closer to the warning time objective: the hypocenter or the centroid.

Sensitivity Maps

To determine the ability of the GeoRED and Escuela Politécnica Nacional (EPN) GNSS networks to detect an earthquake without seismometers, we construct sensitivity maps as shown in

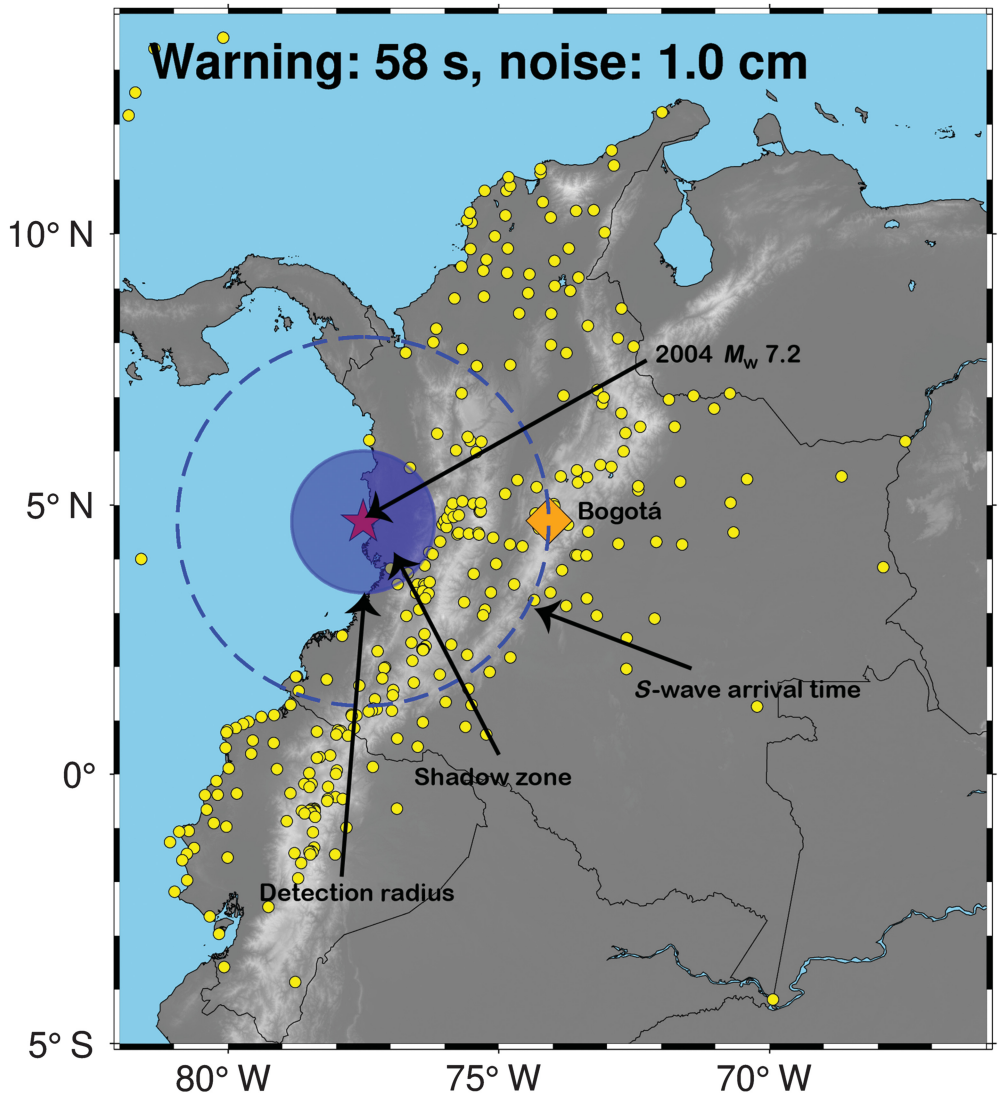

Figure 2. The geometry of an earthquake early warning (EEW) detection and warning event. This figure shows the anatomy of an EEW event; the red star represents the detected epicenter of the event; the blue shaded circle is the shadow zone or the area where seismic *S* waves would propagate before being detected by the minimum number of stations (in this case 4). The outside diameter of the shaded blue area is referred to as the detection radius. The blue dashed line is when the seismic waves would reach the target city. The warning time differs between the detection radius and the blue dashed line. The representative event is the 2004 M_w 7.2, and the warning time would be generated to Bogotá.

Hodgkinson *et al.* (2020) that determine how many stations can detect the long-period dynamic motion from an event at any location, given predicted ambient noise levels and detection threshold models. As an input for this sensitivity map, we use:

- Station locations (latitude and longitude);
- predicted noise levels, σ_{PGD}, of the position estimates for the stations;
- magnitude, M_w, of the hypothetical earthquake for the sensitivity analysis; and
- depth, d, of the hypothetical earthquake for the sensitivity analysis.

For each station location, we determine the "detection" radius for the given magnitude, depth, and noise level. First, we determine a detection threshold for each station based on the noise level. In the case of GeoRED and EPN networks, high-rate data are not currently collected for most GNSS stations, so as a proxy we use the average noise level from the network of the Americas (NOTA) in North America and the Caribbean, which was examined in at least three studies (Hodgkinson *et al.*, 2020; Mattioli *et al.*, 2020; Melgar *et al.*, 2020) and ranges from 0.6 mm to over 1.0 cm—the principal driver of the difference being the different sensitivities of the selected RT-GNSS processing scheme. We use the more conservative value of 1.0 cm. The nominal noise level is typically defined as the standard deviation of the position estimates, σ_{PGD}, calculated within a time window that is relevant to the target detection event. In EEW applications like ShakeAlert, this is calculated using a sliding window (typically 2–15 min) of the calculated horizontal PGD estimates (Hodgkinson *et al.*, 2020; Melgar *et al.*, 2020). We then determine a simple detection threshold model by multiplying a constant, K, times the standard deviation of the noise level, σ_{PGD}, to determine the minimum dynamic motion that a particular station can detect, PGD_{min}. In this study, we consider a K of both 2 and 3. The method used by Hodgkinson *et al.* (2020) used median difference (the difference between the initial position and the median of the sliding window) plus three times the median absolute deviation; in this case, we ignore the median difference, which would give some indication of the long-period detection and the drift of the PGD estimates. This drift varies

TABLE 1
Warning Times (Seconds) for Each City in the Study for Each Earthquake Event Using the Current Network Geometry and Assuming That All Stations Are Functional and Have Real-Time Data Available to the Earthquake Early Warning (EEW) Center

City	1991/11/19 M_w 7.2	2004/11/15 M_w 7.2	1906/01/31 M_w 8.8	1942/05/14 M_w 7.8	1958/01/19 M_w 7.6	2016/04/16 M_w 7.8	1979/12/12 M_w 7.7
Bogotá	53.2	52.3	163.9	190.5	165.8	183.9	145.8
Medellín	29.9	26.2	164.6	193.1	165.4	184.8	142.2
Cali	–0.5	1	88.8	116.4	90.5	109.1	69.7
Barranquilla	152.9	147.5	289.6	317.8	289.6	308.8	265.3
Cartagena	130.6	125	266.7	294.7	266.6	285.6	242.2
Tumaco	44.4	44.5	13.1	41.6	14.2	33.3	–6.5
Guayaquil	158.6	159.2	72.5	42.7	73.9	53.7	81.9
Quito	83.6	84.4	15.4	22.6	19.2	21.7	20.7
Esmeraldas	76.6	76.4	–8	9.5	–10.4	0.3	–4.6
Ibarra	77.6	78.6	22.2	33.7	26.1	32	24.1
Tulcán	63.9	65	30	48	33.7	44.6	26.3
Riobamba	135.6	136.6	59.7	41.1	62.4	49.4	68.6

from 7 to 8.5 mm over periods from 10 s to 10 min (Hodgkinson *et al.*, 2020).

We define a minimum PGD detection threshold

$$\mathrm{PGD}_{\min} = K \times \sigma_{\mathrm{PGD}}, \tag{1}$$

we then calculate a detection radius for each station using the empirical formulas of Wu and Zhao (2006), Crowell *et al.* (2013), Melgar *et al.* (2015), and Ruhl *et al.* (2018),

$$\log(\mathrm{PGD}) = A + B \times M_w + C \times M_w \times \log(R), \tag{2}$$

in which A, B, and C are empirically derived constants. M_w is the magnitude of the earthquake. R is the hypocentral distance from the earthquake.

We solve for R and substitute $\mathrm{PGD}_{\min}$ for PGD:

$$R = \left(\frac{\log(\mathrm{PGD}_{\min}) - A - B \times M_w}{C \times M_w}\right)^{10}, \tag{3}$$

in which R is now the detection radius for a given station. A, B, and C are empirically derived constants. M_w is the magnitude of the earthquake.

We then construct a sensitivity map by calculating the number of stations that would detect an earthquake of size, M_w, by counting the number of overlapping detection radii for all the stations at a given earthquake origin location. Or stated another way, this overlap, or station detection density, represents the number of stations that would detect an earthquake of size, M_w, at that location. We further apply a constraint that a minimum number of stations, min, must detect the earthquake, that is, we cannot issue an early warning based on one station (Cochran *et al.*, 2017; Kohler *et al.*, 2017). We eliminate any location that does not meet this minimum threshold from the sensitivity map. All the sensitivity maps in this study use empirical constants (A, B, and C) from Melgar *et al.* (2015).

Warning Times

Although sensitivity maps give an overall picture of the "detectability" of an earthquake, they do not give a picture of the ability of the system to issue a reasonable warning based on a detected event. EEW systems rely on the immediate detection of an event and then use modern communication systems to leap-frog in front of the destructive ground motion and issue a warning that the arrival of this ground motion is imminent. This means that EEW systems are largely dependent on how close the initial stations are to the origin of the earthquake and subsequent rupture, and how far away the population or infrastructure is from this point. In addition, we assume that the detection is required at several stations before enough confidence is gained to issue a warning and characterize the magnitude of the earthquake (Cochran *et al.*, 2017; Kohler *et al.*, 2020). The distance (or time) it takes for the energy to be detected on the minimum number of sensors is called the shadow zone and is the area where no warning can be issued (Fig. 2). The warning time is then the time it takes for this energy to travel from the time of

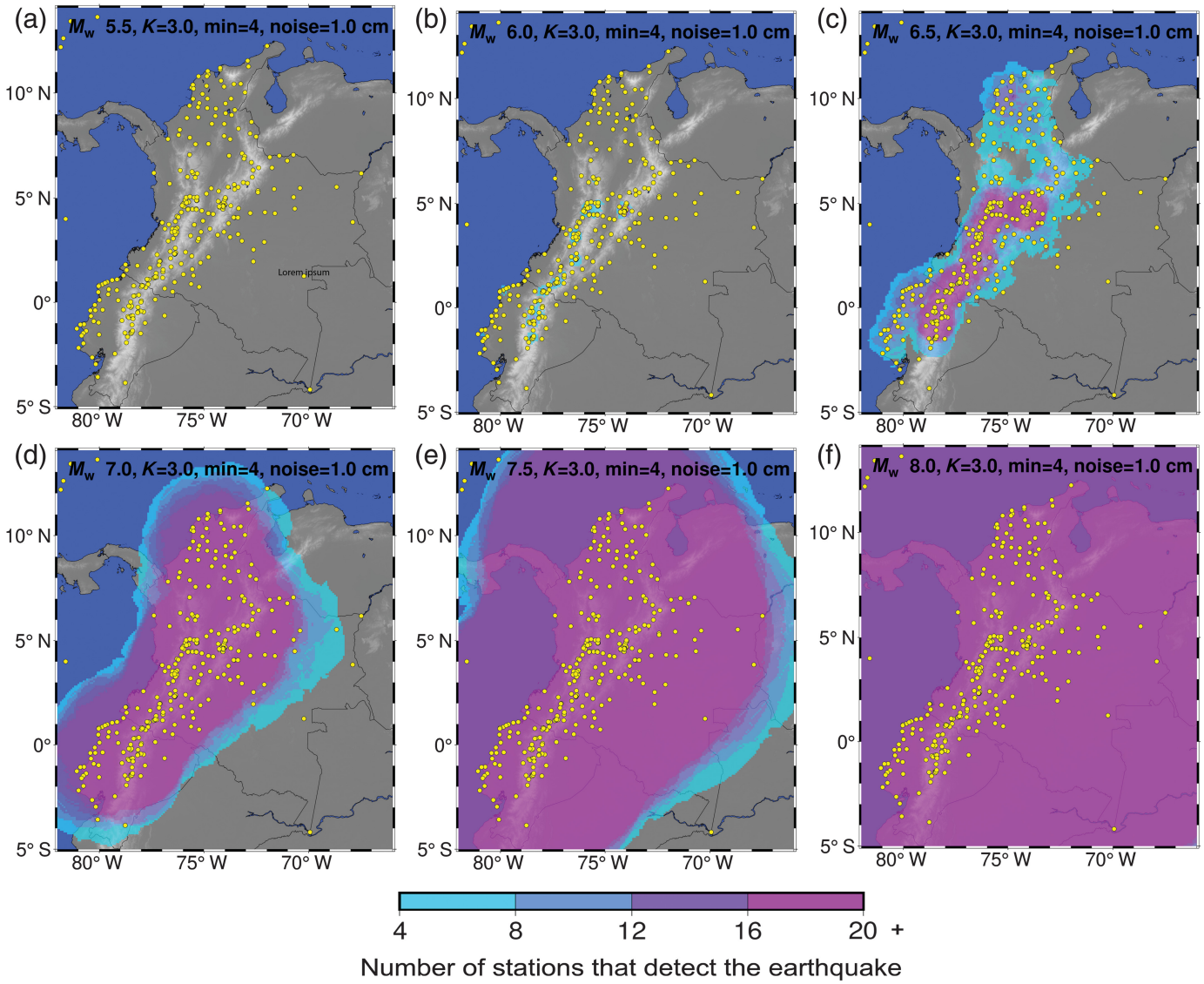

Figure 3. Sensitivity maps of the network for (a–f) M_w 5.5–8.0 events in 0.5 M increments and a noise detection model of three times the predicted noise level, σ_{PGD}, or K = 3. In general, the sensitivity is good for any event equal to or larger than an M_w 7, but these sensitivity maps do not represent what warning times would be generated for any individual event. Comparing this with Figure 4 shows the dependence of the sensitivity to noise.

detection to the location that the warning is desired minus any processing and communication travel time (typically less than 10 s). For this study, we use seven large historical events from the Pacific subduction zone (Pulido *et al.*, 2020) and generate warning times for major or critical population centers (Table 1) in Colombia and Ecuador showing what would have been possible had the system been operational using the current geometry at that time. Large earthquakes have large and complex rupture patterns, while we treat these earthquakes as point sources in this study, we consider this as a reasonable proxy as the initial detection and warning typically rapidly converge (Crowell *et al.*, 2009; Cochran *et al.*, 2017; Kohler *et al.*, 2020). Although EEW has limited utility in situations where the population center sits directly on or adjacent to the rupture hazard (e.g., Cartagena sits on top of a seismic hazard that is capable of M_w 8+ events, Mencin, 2018; Lizarazo *et al.*, 2021), both Colombia and Ecuador present ideal geometries where large population centers sit several 100 km inland from the seismogenic source. EEW still retains some utility for locations like Cartagena because it can be used to rapidly characterize any generated tsunamis. The seven historical earthquakes used in this study generate a predicted PGD between ~2 and 800 cm that would have occurred at the target cities, all detectable with current algorithms. Some of these earthquakes induced considerable damage and loss of life in cities farther inland from the event (Pulido *et al.*, 2020).

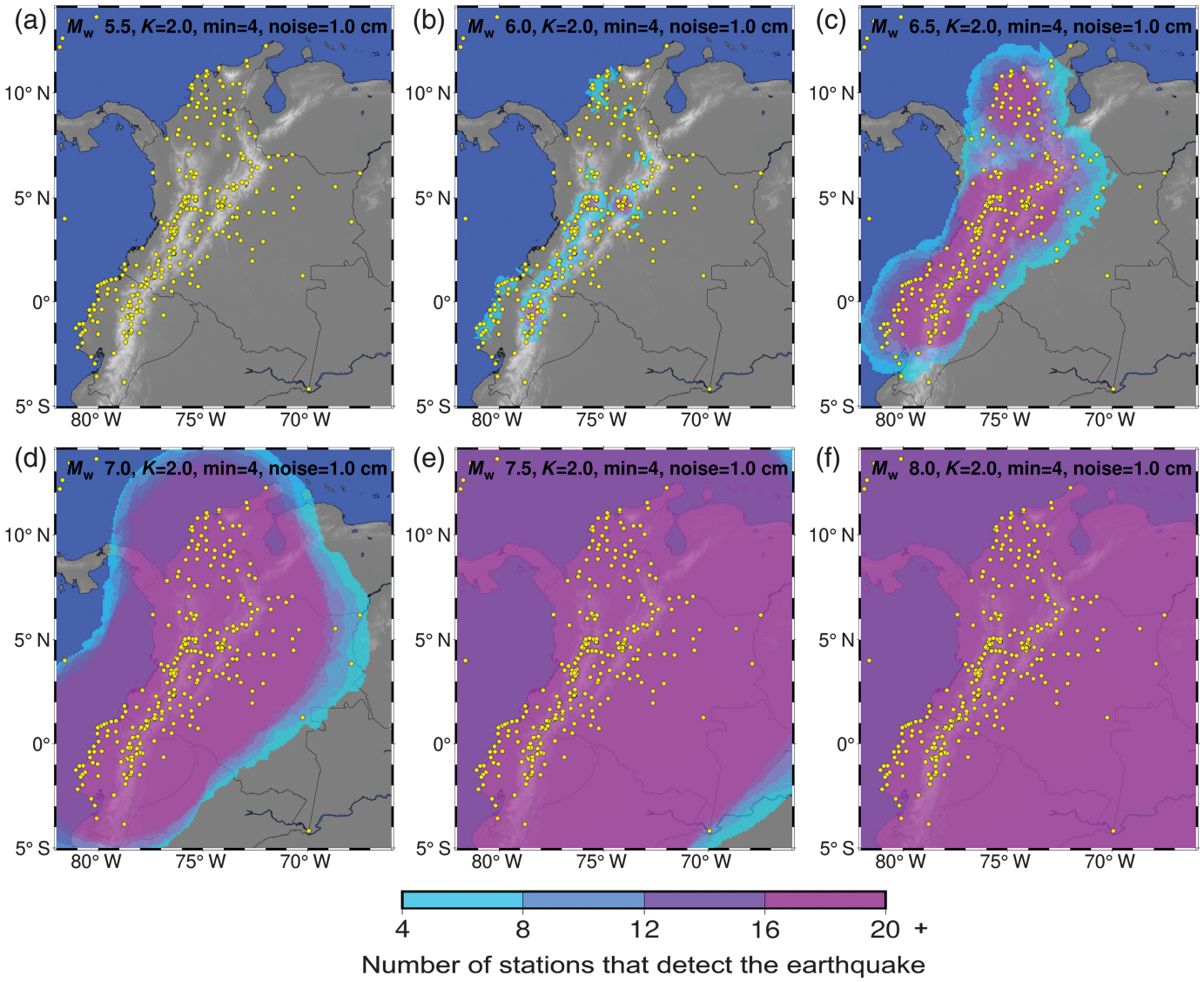

Figure 4. Sensitivity maps of the network for (a–f) M_w 5.5–8.0 events in 0.5 M increments and a noise detection model of two times the predicted noise level, σ_{PGD}, or K = 2. In general, the sensitivity is good for any event equal to or larger than an M_w 6.5 (with K = 2), but these sensitivity maps do not represent what warning times would be generated for any particular event.

Analysis

Given the sparse existing seismic networks and the already existing geodetic GNSS infrastructure, we analyze a network that is based solely on GNSS (Grapenthin *et al.*, 2017).

Colombia, and to a degree Ecuador, are ideal for a GNSS-based EEW system in that large, moderate-depth subduction zone earthquakes occur frequently 100's of kilometers away from large metropolitan areas and critical infrastructure—a geometry that allows for reasonable warning times. Figures 3 and 4 show current network sensitivity to M_w 5.5–8.0 event in 0.5 M increments for different noise detection models, K = 2 and K = 3, and the minimum number of stations that detect the event required to issue a warning set to four. The current geometry has excellent sensitivity for events larger than M_w 7.0, although the sensitivity maps do not do well in highlighting the deficiencies of the current network in an EEW application as the overall sensitivity, assuming all the stations have reliable communications, is very good. In terms of the warning times, in many cases the current network performs reasonably well, especially for earthquakes that are located offshore of Ecuador where there is an excellent distribution of GNSS stations along the shoreline, and detection is rapid, allowing for maximum possible warning times (Fig. 1). The 1906 M_w 8.8 that occurred near the border of Colombia and Ecuador would have given Cali and Quito 88 s and 15 s warning time, respectively (Table 1). We calculate the warning time for twelve metropolitan areas chosen either for size or critical infrastructure for each of the historical earthquakes (Table 1) as well as the shadow

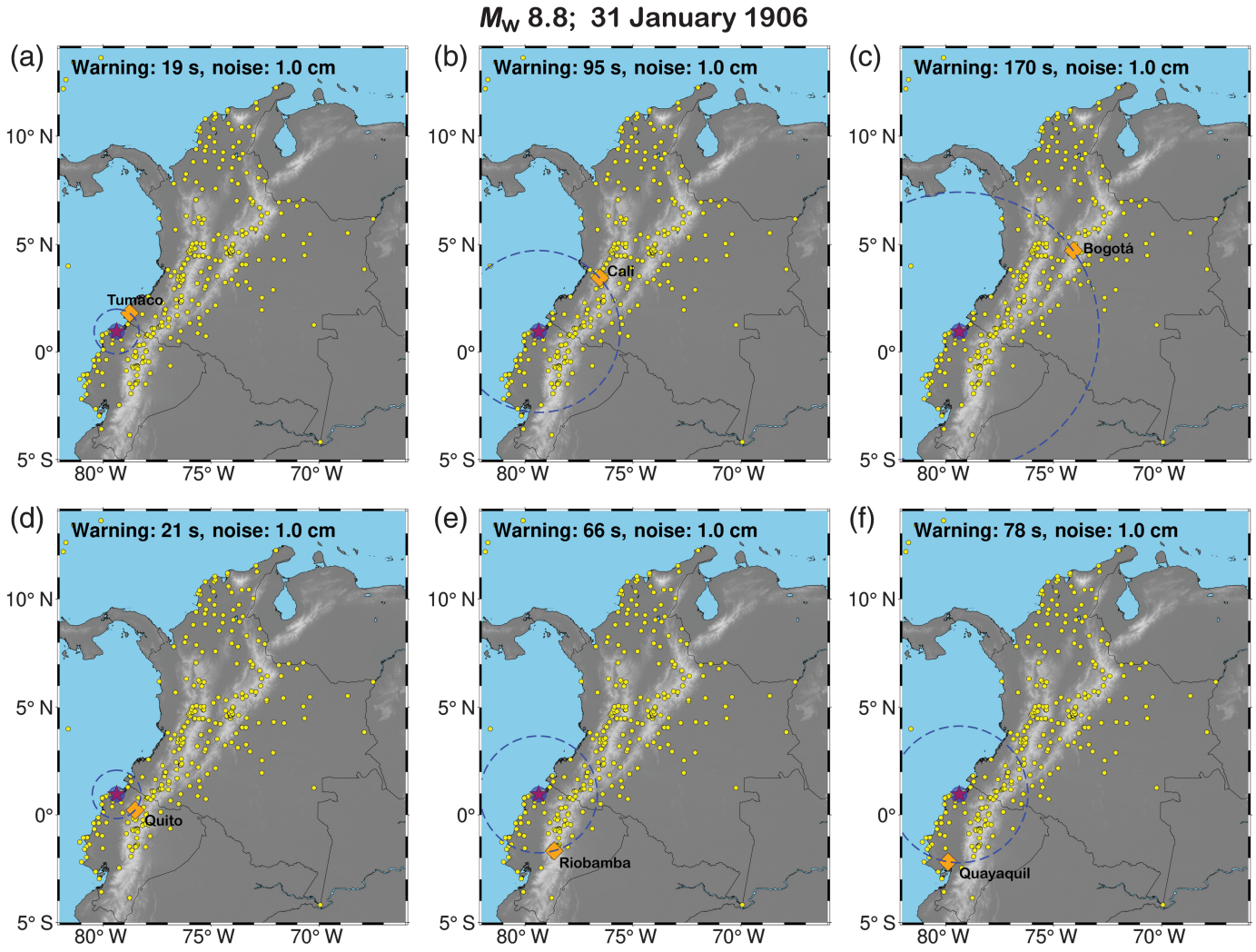

Figure 5. Graphical representation of an EEW event for the 1906 M_w 8.8, which created widespread damage throughout Colombia and Ecuador (Pulido *et al.*, 2020) for (a–f) six major and/or important metropolitan areas: three in Colombia and three in Ecuador. The current GNSS network geometry in Ecuador would allow the best possible warning times for this event.

zone radius for each event, which gives some indication if the existing geometry is optimal for detecting that event (Table 2). In addition, we graphically represent the EEW for two events: the 1906 M_w 8.8 earthquake, which created widespread damage throughout Colombia and Ecuador (Pulido *et al.*, 2020), and the 2004 M_w 7.2 event, which is representative of where the network geometry is poor for six major and/or important metropolitan areas: three in Colombia and three in Ecuador in Figures 5 and 6. The travel time in these calculations assumes a propagation velocity of 4 km/s, that it will take 6 s to process and detect a warning, and that four stations are required to detect an event before a warning can be issued. We note that some cities have negative warning times, simply indicating that the detection and warning would happen after the destructive waves have already passed that location. These situations highlight either a deficiency in the current geometry or the fact that earthquake is simply too close to allow for any reasonable warning to be issued (Minson *et al.*, 2018).

Table 1 shows that in many cases ample warning times can be issued using the current geometry. The primary deficiencies in the current network configuration in terms of EEW are the lack of stations along the Colombian Pacific Coast. It is obvious that the current GNSS network geometry in Ecuador would allow the best possible warning times for large events that occur on the subduction interface between the Nazca and South American plates.

Modifications and Improvements to the Network

To build an ideal EEW network that minimizes shadow zones and allows for maximum warning times as constrained by network geometry, we analyze several scenarios. We do this

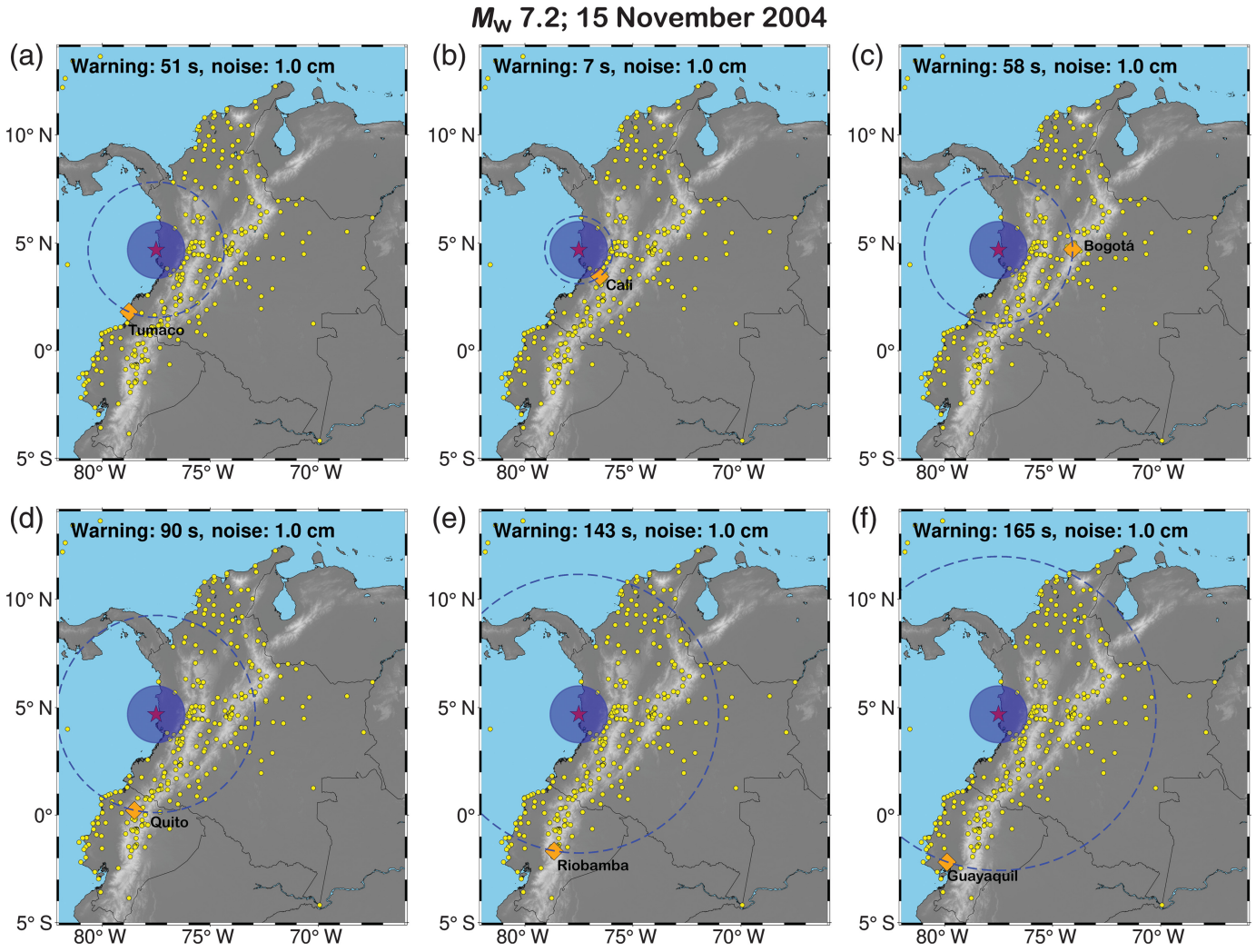

Figure 6. Graphical representation of an EEW event for the 2004 M_w 7.2, which is a representative event for where there is poor network coverage for (a–f) six major and/or important metropolitan areas: three in Colombia and three in Ecuador.

TABLE 2
Blindspot Radius (Kilometer) for the Seven Earthquakes Used in This Study

Date (yyyy/mm/dd)	M_w	Current	100 km	50 km	25 km
1991/11/19	7.2	135.97	85.92	50.07	29.92
2004/11/15	7.2	146.71	80.61	54.45	36.99
1906/01/31	8.8	39.45	39.45	39.45	39.45
1942/05/14	7.8	49.84	49.84	49.84	49.84
1958/01/19	7.6	37.5	37.5	37.5	37.5
2016/04/16	7.8	46.15	46.15	46.15	46.15
1979/12/12	7.7	71.19	64.3	61.91	58.27

Shadow zones are independent of the city and are the same for all scenarios. Shadow zones give an indication of the strength of the network geometry; larger shadow zones may indicate poor or sparse geometry.

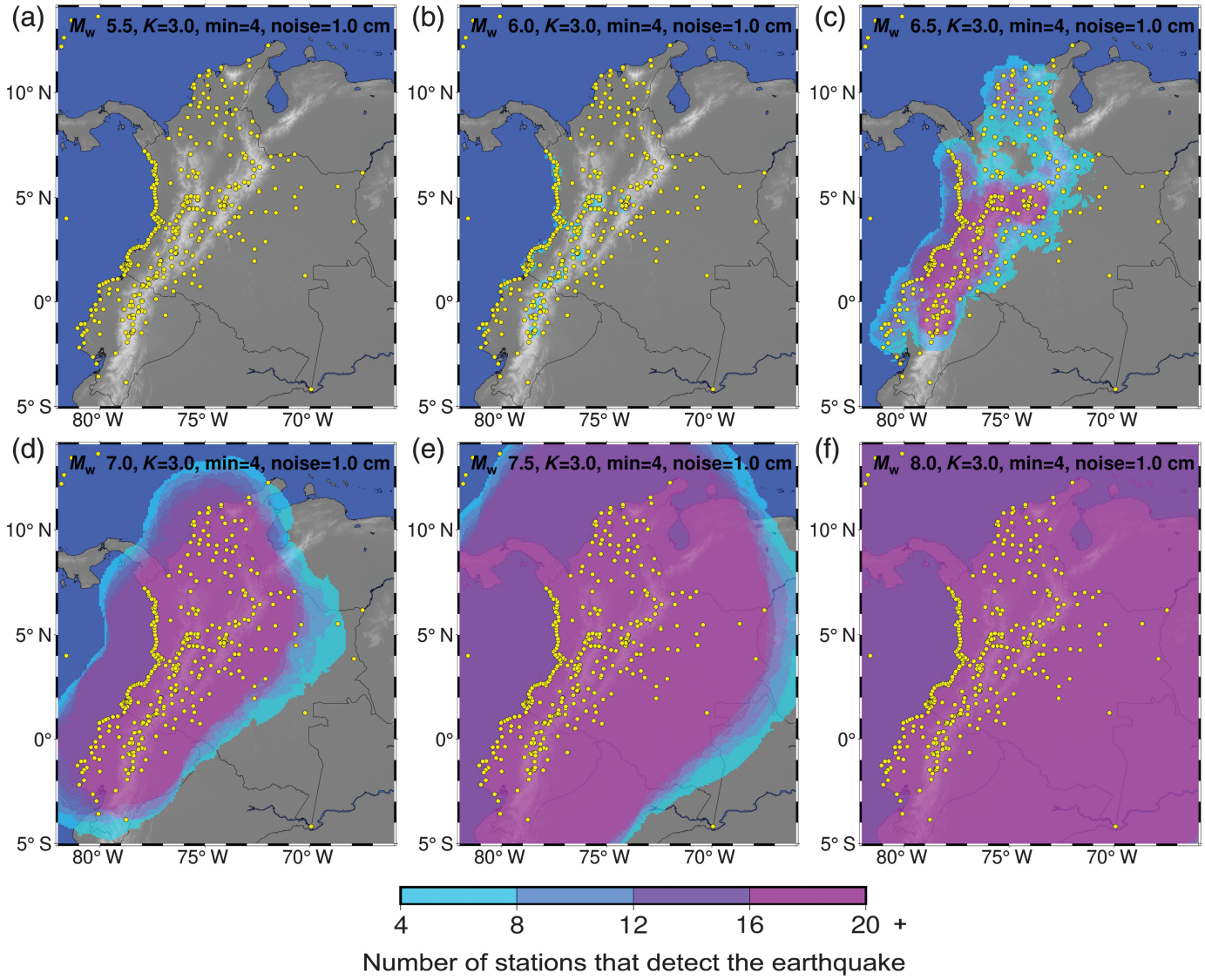

Figure 7. Sensitivity maps of the network for (a–f) M_w 5.5–8.0 events in 0.5 M increments and a noise detection model of three times the predicted noise level, σ_{PGD}, or K = 3. This scenario uses a hypothetical line of "Sentinel" stations along the Pacific coast of Colombia with 25 km spacing. These sentinel stations reduce the sensitivity floor to near M_w 6. Comparing this with Figure 8 shows the dependence of the sensitivity to noise.

by adding "sentinel" stations along the Colombian Pacific coast with regular spacing (we ignore the obvious siting, permitting, and infrastructure issues that would be involved) of 25, 50, and 100 km, which would require the addition of 67, 34, and 18 new GNSS stations, respectively. As discussed earlier, the obvious weak spot in the current geometry for protection against earthquakes in the subduction interface between the Nazca and South American plates is here. This configuration of "sentinel" stations—those stations as close as possible to the seismogenic portion of the subduction zone where large and destructive earthquakes occur allows for rapid detection and minimal shadow zones. In Figures 7 and 8, we reconstruct the sensitivity maps with the same noise detection thresholds used for the existing network geometries. There are notable improvements along the Pacific Coast of Colombia in terms of sensitivity. The improvements that make an investment like this worthwhile are illustrated in Figures 9 and 10, Tables 2 and 3. As an example, in the existing geometry, an earthquake like the 2004 M_w 7.2 event, with the 25 km spacing scenario, increases the warning time for Cali from 3 to 30 s—this later time giving ample warning for viable reactions. Three seconds is arguably not enough time for anything but a fully automated response, like those on trains or critical infrastructure like gas and water lines, whereas 30 seconds is ample time for a public warning. Cali is a large critical metropolitan area in Colombia.

In addition to the added warning time an augmentation like this would provide to some coastal cities in Colombia, GNSS

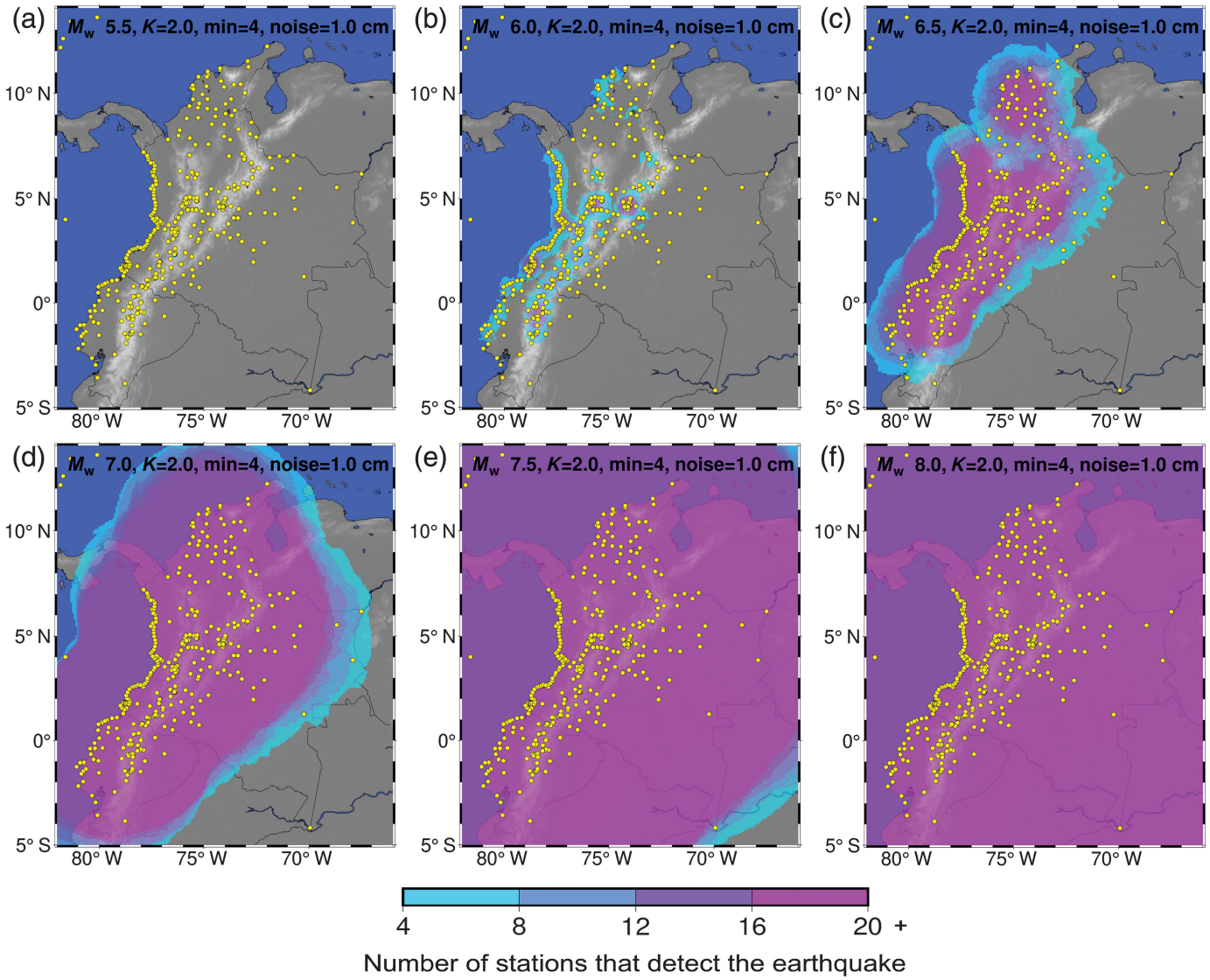

Figure 8. Sensitivity maps of the network for (a–f) M_w 5.5–8.0 events in 0.5 M increments and a noise detection model of two times the predicted noise level, σ_{PGD}, or $K = 2$. This scenario uses a hypothetical line of "Sentinel" stations along the Pacific coast of Colombia with 25 km spacing. These sentinel stations reduce the sensitivity floor to at least M6.5.

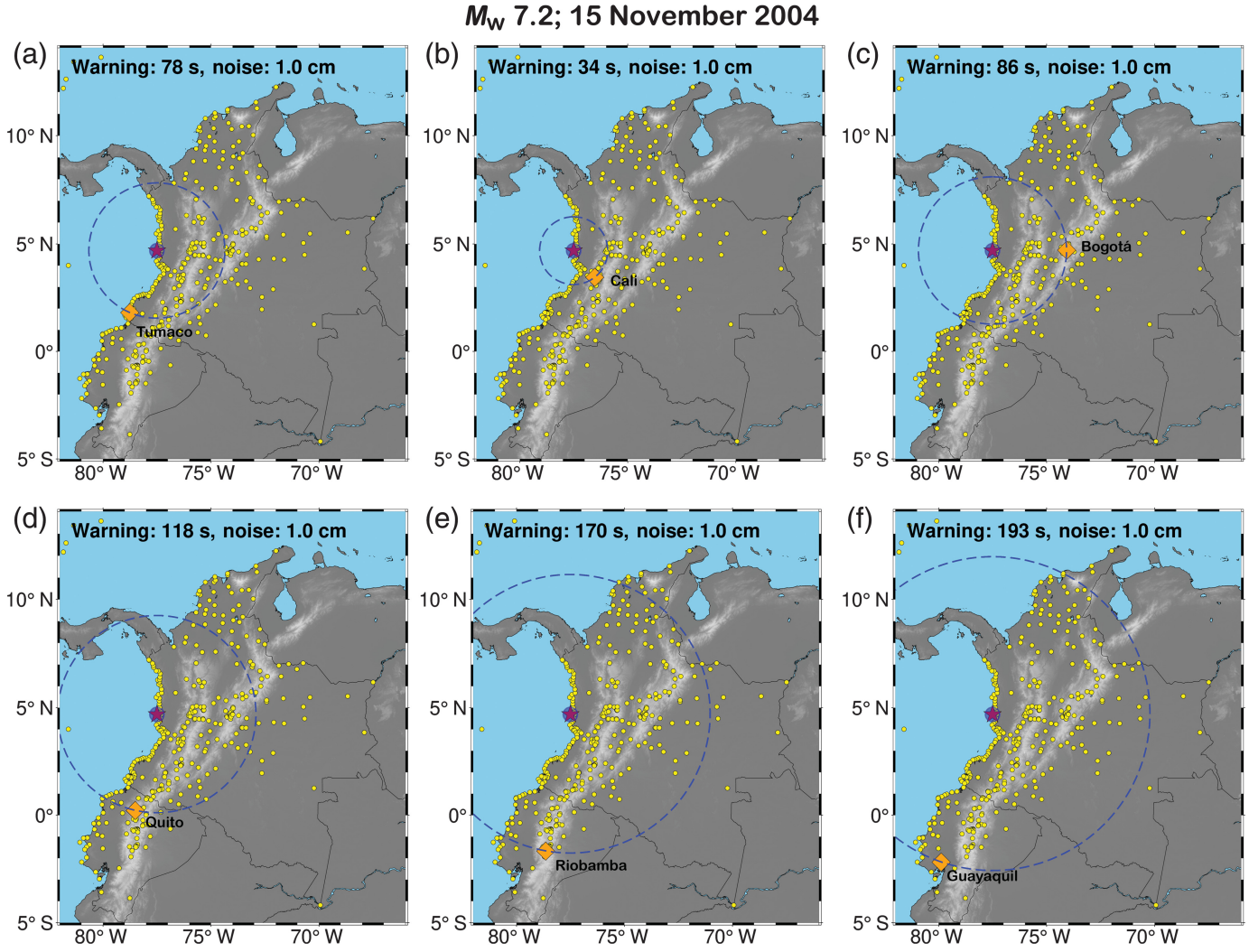

Figure 9. Graphical representation of an EEW event for the 2004 M_w 7.2, which is a representative event for where there is poor current network coverage, for (a–f) six major and/or important metropolitan areas: three in Colombia and three in Ecuador. This scenario is using a hypothetical line of "Sentinel" stations along the Pacific coast of Colombia with 25 km spacing, markedly improving the warning times.

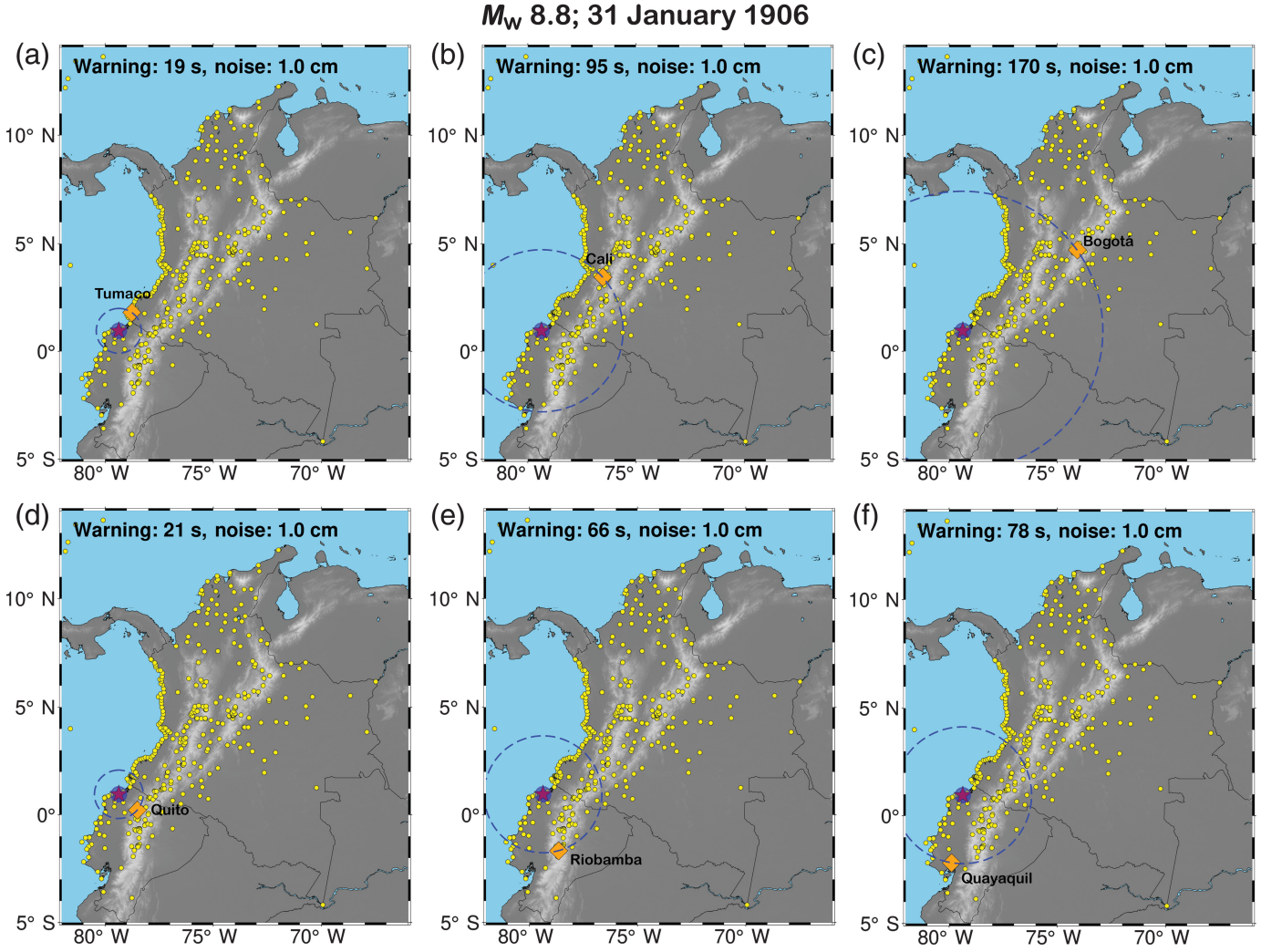

Figure 10. Graphical representation of an EEW event for the 1906 M_W 8.8, which created widespread damage throughout Colombia and Ecuador (Pulido *et al.*, 2020) for (a–f) six major and/or important metropolitan areas: three in Colombia and three in Ecuador. This scenario uses a hypothetical line of "Sentinel" stations along the Pacific coast of Colombia with 25 km spacing.

TABLE 3
Warning Times (Seconds) for Each City in the Study for Each Earthquake Event Using the Network Geometry That Includes Sentinel Stations along the Colombian Pacific Coast with a Spacing of 25 km and Assuming That All Stations Are Functional and Have Real-Time Data Available to the Earthquake Early Warning (EEW) Center

City	1991/11/19 M_w 7.2	2004/11/15 M_w 7.2	1906/01/31 M_w 8.8	1942/05/14 M_w 7.8	1958/01/19 M_w 7.6	2016/04/16 M_w 7.8	1979/12/12 M_w 7.7
Bogotá	79.7	79.7	163.9	190.5	165.8	183.9	149
Medellín	56.4	53.6	164.6	193.1	165.4	184.8	145.5
Cali	26	28.4	88.8	116.4	90.5	109.1	72.9
Barranquilla	179.4	174.9	289.6	317.8	289.6	308.8	268.5
Cartagena	157.1	152.4	266.7	294.7	266.6	285.6	245.4
Tumaco	70.9	72	13.1	41.6	14.2	33.3	–3.3
Guayaquil	185.2	186.6	72.5	42.7	73.9	53.7	85.2
Quito	110.1	111.8	15.4	22.6	19.2	21.7	23.9
Esmeraldas	103.1	103.9	–8	9.5	–10.4	0.3	–1.4
Ibarra	104.1	106	22.2	33.7	26.1	32	27.3
Tulcán	90.4	92.5	30	48	33.7	44.6	29.5
Riobamba	162.1	164	59.7	41.1	62.4	49.4	71.9

stations along the coast could serve multiple other roles: tsunami estimation and detection (Angove *et al.*, 2019; Mori *et al.*, 2022), tsunami detection using ionospheric disturbance detection (Savastano *et al.*, 2017; Ravanelli *et al.*, 2021), sea level change (Peng *et al.*, 2021), and other GNSS interferometric reflectometry (GNSS-IR) applications (Larson, 2019). Ecuador already has a well-developed GNSS network along the coast. These sentinel stations significantly improve warning times, in some cases, and allow for reasonable warning times in large metropolitan areas that are not possible with the existing geometry and current real-time communications.

Conclusions

Colombia and Ecuador have existing GNSS infrastructure that could be utilized as is for an EEW system with modest upgrades to communications. Given the sparse seismic network that exists in Colombia, triggering will have to wholly or partially be based on GNSS data alone (Grapenthin *et al.*, 2017). The most significant deficiency in the defense of large subduction zone earthquakes along the Pacific Coast is the lack of coastal or sentinel stations along the Pacific coast of Colombia. We analyzed three scenarios of placing GNSS stations at spacing intervals of 25, 50, and 100 km along the Colombian Pacific Coast to quantitatively assess the improvement that could be realized in building this network out. We show significant improvement times for several cities, most notably Cali, with the addition of these stations (Table 3). We conclude the following improvements in priority order:

- Improve and harden communications to all the GNSS stations, with a priority to those stations within 100 km of the Pacific Coast. This is essential to transform the existing GNSS infrastructure into a viable EEW system.
- Invest in cloud-based skills and infrastructure, preferably in-country, to develop, operate, and maintain a viable EEW system. Software and methods could be adopted from existing operational systems like those in the United States operated by the USGS and EarthScope for North America and the pan-Caribbean region.
- Installation of sentinel stations along the Pacific Coast in Colombia, starting with 100 km spacing and progressively moving toward 25 km spacing. This will allow for maximum benefits in the least amount of time.
- Although Ecuador appears to have a sufficiently dense seismic network for triggering, an analysis is needed; Colombia would benefit from a dense seismic network. This would be a significant investment with considerable payback in terms of science. Benefits for EEW would be limited to increased sensitivity, but these have real benefits in terms of acceptance and utilization of issued warnings—an important aspect of EEW.
- We believe these suggested improvements offer the lowest cost path to a viable EEW system in Colombia and Ecuador.

We also note it is essential that EEW systems are regional in nature; large destructive earthquakes do not recognize political boundaries and can occur near but outside a country's political border. Rapid and open exchange of

solutions is essential to the viable operation of EEW systems. A final recommendation is to expand the network to neighboring countries.

Data and Resources

Maps were made using the Generic Mapping Tools (GMT) version 6 (Wessel and Luis, 2017) and the PyGMT wrapper (Tian *et al.*, 2024). The NumPy package is part of the Python open-source mathematics library (Harris *et al.*, 2020). The PANDAS package is available on Zenodo and at pandas.pydata.org (last accessed May 2024) (The pandas development team, 2024).

Declaration of Competing Interests

The authors acknowledge that there are no conflicts of interest recorded.

Acknowledgments

This work was supported in part by the Servicio Geológico Colombiano and National Science Foundation (NSF) OAC-1835791.

References

Acosta, J., F. Velandia, J. Osorio, L. Lonergan, and H. Mora (2007). Strike-slip deformation within the Colombian Andes, *Geol. Soc. Lond. Spec. Publ.* **272,** no. 1, 303–319, doi: 10.1144/gsl.sp.2007.272.01.16.

Allen, R. M., and D. Melgar (2019). Earthquake early warning: Advances, scientific challenges, and societal needs, *Annu. Rev. Earth Planet. Sci.* **47,** no. 1, 1–28, doi: 10.1146/annurev-earth-053018-060457.

Alvarado, A., M. Ruiz, P. Mothes, H. Yepes, M. Segovia, M. Vaca, C. Ramos, W. Enríquez, G. Ponce, P. Jarrín, *et al.* (2018). Seismic, volcanic, and geodetic networks in Ecuador: Building capacity for monitoring and research, *Seismol. Res. Lett.* **89,** no. 2A, 432–439, doi: 10.1785/0220170229.

Angove, M., D. Arcas, R. Bailey, P. Carrasco, D. Coetzee, B. Fry, K. Gledhill, S. Harada, C. von Hillebrandt-Andrade, L. Kong, *et al.* (2019). Ocean observations required to minimize uncertainty in global tsunami forecasts, Warnings, and emergency response, *Front. Mar. Sci.* **6,** 350, doi: 10.3389/fmars.2019.00350.

Bilham, R., and D. Mencin (2013). Potential for great thrust earthquakes in NE Colombia & NW Venezuela, in *AGU Spring Meeting Abstracts*, Cancún Center, Cancún, Mexico, 13–17 May 2013, T21A-01.

Bird, P. (2003). An updated digital model of plate boundaries, *Geochem. Geophys. Geosyst.* **4,** no. 3, doi: 10.1029/2001gc000252.

Böse, M., D. E. Smith, C. Felizardo, M.-A. Meier, T. H. Heaton, and J. F. Clinton (2017). FinDer v.2: Improved real-time ground-motion predictions for M2–M9 with seismic finite-source characterization, *Geophys. J. Int.* **212,** no. 1, 725–742, doi: 10.1093/gji/ggx430.

Chung, A. I., I. Henson, and R. M. Allen (2019). Optimizing earthquake early warning performance: ElarmS-3, *Seismol. Res. Lett.* **90,** no. 2A, 727–743, doi: 10.1785/0220180192.

Cochran, E. S., M. D. Kohler, D. D. Given, S. Guiwits, J. Andrews, M. A. Meier, M. Ahmad, I. Henson, R. Hartog, and D. Smith (2017). Earthquake early warning ShakeAlert system: Testing and certification platform, *Seismol. Res. Lett.* **89,** no. 1, 108–117, doi: 10.1785/0220170138.

Crowell, B. W., Y. Bock, and M. B. Squibb (2009). Demonstration of earthquake early warning using total displacement waveforms from real-time GPS networks, *Seismol. Res. Lett.* **80,** no. 5, 772–782, doi: 10.1785/gssrl.80.5.772.

Crowell, B. W., D. Melgar, Y. Bock, J. S. Haase, and J. Geng (2013). Earthquake magnitude scaling using seismogeodetic data, *Geophys. Res. Lett.* **40,** no. 23, 6089–6094, doi: 10.1002/2013gl058391.

Crowell, B. W., D. A. Schmidt, P. Bodin, J. E. Vidale, B. Baker, S. Barrientos, and J. Geng (2018). G-FAST earthquake early warning potential for Great Earthquakes in Chile, *Seismol. Res. Lett.* **89,** no. 2A, 542–556, doi: 10.1785/0220170180.

Dittmann, T., K. Hodgkinson, J. Morton, D. Mencin, and G. S. Mattioli (2022). Comparing sensitivities of geodetic processing methods for rapid earthquake magnitude estimation, *Seismol. Res. Lett.* **93,** no. 3, 1497–1509, doi: 10.1785/0220210265.

Dittmann, T., Y. Liu, Y. Morton, and D. Mencin (2022). Supervised machine learning of high rate GNSS velocities for earthquake strong motion signals, *J. Geophys. Res.* **127,** no. 11, doi: 10.1029/2022jb024854.

Freymueller, J. T., J. N. Kellogg, and V. Vega (1993). Plate motions in the north Andean region, *J. Geophys. Res (1978–2012)* **98,** no. B12, 21,853–21,863, doi: 10.1029/93jb00520.

Given, D. (2014). Technical implementation plan for the ShakeAlert production system—An earthquake early warning system for the West Coast of the United States, *U.S. Geol. Surv. Open-File Rept. 2014–1097*, 1–31, doi: 10.3133/ofr20141097.

Given, D. D. (2018). Revised technical implementation plan for the ShakeAlert system—An earthquake early warning system for the West Coast of the United States, *Open-File Rept. 2018-1155*, 1–54, doi: 10.3133/ofr20181155.

Grapenthin, R., M. West, and J. Freymueller (2017). The utility of GNSS for earthquake early warning in regions with sparse seismic networks, *Bull. Seismol. Soc. Am.* **107,** no. 4, 1883–1890, doi: 10.1785/0120160317.

Harris, C. R., K. J. Millman, S. J. van der Walt, R. Gommers, P. Virtanen, D. Cournapeau, E. Wieser, J. Taylor, S. Berg, N. J. Smith, *et al.* (2020). Array programming with NumPy, *Nature* **585,** no. 7825, 357–362, doi: 10.1038/s41586-020-2649-2.

Hodgkinson, K. M., D. J. Mencin, K. Feaux, C. Sievers, and G. S. Mattioli (2020). Evaluation of earthquake magnitude estimation and event detection thresholds for real-time GNSS networks: Examples from recent events captured by the network of the Americas, *Seismol. Res. Lett.* **91,** no. 3, 1628–1645, doi: 10.1785/0220190269.

Hossen, M. J., I. E. Mulia, D. Mencin, and A. F. Sheehan (2021). Data assimilation for tsunami forecast with ship-borne GNSS data in the Cascadia subduction zone, *Earth Space Sci.* **8,** no. 3, doi: 10.1029/2020ea001390.

Kohler, M. D., E. S. Cochran, D. Given, S. Guiwits, D. Neuhauser, I. Henson, R. Hartog, P. Bodin, V. Kress, S. Thompson, *et al.* (2017). Earthquake early warning ShakeAlert system: West Coast wide production prototype, *Seismol. Res. Lett.* **89,** no. 1, 99–107, doi: 10.1785/0220170140.

Kohler, M. D., D. E. Smith, J. Andrews, A. I. Chung, R. Hartog, I. Henson, D. D. Given, R. de Groot, and S. Guiwits (2020). Earthquake early warning ShakeAlert 2.0: Public rollout, *Seismol. Res. Lett.* 1–13, doi: 10.1785/0220190245.

Larson, K. M. (2019). Unanticipated uses of the Global Positioning System, *Annu. Rev. Earth Planet. Sci.* **47,** no. 1, 19–40, doi: 10.1146/annurev-earth-053018-060203.

Lizarazo, S. C., T. Sagiya, and H. Mora-Páez (2021). Interplate coupling along the Caribbean coast of Colombia and its implications for seismic/tsunami hazards, *J. Soc. Am. Earth Sci.* **110,** 103332, doi: 10.1016/j.jsames.2021.103332.

Mattioli, G. S., D. A. Phillips, K. M. Hodgkinson, C. Walls, D. J. Mencin, B. A. Bartel, D. J. Charlevoix, C. Crosby, M. J. Gottlieb, B. Henderson, *et al.* (2020). The GAGE data and field response to the 2019 Ridgecrest earthquake sequence, *Seismol. Res. Lett.* **91,** no. 4, 1–12, doi: 10.1785/0220190283.

Melgar, D., R. M. Allen, S. Riquelme, J. Geng, F. Bravo, J. C. Baez, H. Parra, S. Barrientos, P. Fang, Y. Bock, *et al.* (2016). Local tsunami warnings: Perspectives from recent large events, *Geophys. Res. Lett.* **43,** no. 3, 1109–1117, doi: 10.1002/2015gl067100.

Melgar, D., B. W. Crowell, J. Geng, R. M. Allen, Y. Bock, S. Riquelme, E. M. Hill, M. Protti, and A. Ganas (2015). Earthquake magnitude calculation without saturation from the scaling of peak ground displacement, *Geophys. Res. Lett.* **42,** no. 13, 5197–5205, doi: 10.1002/2015gl064278.

Melgar, D., B. W. Crowell, T. I. Melbourne, W. Szeliga, M. Santillan, and C. Scrivner (2020). Noise characteristics of operational real-time high-rate GNSS positions in a large aperture network, *J. Geophys. Res.* **125,** no. 7, 163–15, doi: 10.1029/2019jb019197.

Mencin, D. J. (2018). *Periodic and Static Strain Investigations with Borehole Strainmeters and GPS*, University of Colorado, Boulder, Colorado.

Minson, S. E., M. A. Meier, A. S. Baltay, T. C. Hanks, and E. S. Cochran (2018). The limits of earthquake early warning: Timeliness of ground motion estimates, *Sci. Adv.* **4,** no. 3, eaaq0504, doi: 10.1126/sciadv.aaq0504.

Mora-Páez, H., J. N. Kellogg, J. T. Freymueller, D. Mencin, R. M. S. Fernandes, H. Diederix, P. LaFemina, L. C. Piedrahita, S. Lizarazo, J. R. P. Gaviria, *et al.* (2018). Crustal deformation in the northern Andes—A new GPS velocity field, *J. South Am. Earth Sci.* **89,** 76–91, doi: 10.1016/j.jsames.2018.11.002.

Mori, N., K. Satake, D. Cox, K. Goda, P. A. Catalan, T.-C. Ho, F. Imamura, T. Tomiczek, P. Lynett, T. Miyashita, *et al.* (2022). Giant tsunami monitoring, early warning and hazard assessment, *Nat. Rev. Earth Environ.* **3,** no. 9, 557–572, doi: 10.1038/s43017-022-00327-3.

Murray, J. R., B. W. Crowell, R. Grapenthin, K. Hodgkinson, J. O. Langbein, T. Melbourne, D. Melgar, S. E. Minson, and D. A. Schmidt (2018). Development of a geodetic component for the U.S. West Coast earthquake early warning system, *Seismol. Res. Lett.* **89,** no. 6, 1–15, doi: 10.1785/0220180162.

Murray, J. R., B. W. Crowell, M. H. Murray, C. W. Ulberg, J. J. McGuire, M. A. Aranha, and M. T. Hagerty (2023). Incorporation of real-time earthquake magnitudes estimated via peak ground displacement scaling in the ShakeAlert earthquake early warning system, *Bull. Seismol. Soc. Am.* **113,** no. 3, 1286–1310, doi: 10.1785/0120220181.

Peng, D., L. Feng, K. M. Larson, and E. M. Hill (2021). Measuring coastal absolute sea-level changes using GNSS Interferometric Reflectometry, *Remote Sens.* **13,** no. 21, 4319, doi: 10.3390/rs13214319.

Pulido, N., M. Yoshimoto, and A. M. Sarabia (2020). Broadband wavelength slip model of the 1906 Ecuador-Colombia megathrust-earthquake based on seismic intensity and tsunami data, *Tectonophysics* **774,** 228226, doi: 10.1016/j.tecto.2019.228226.

Ravanelli, M., G. Occhipinti, G. Savastano, A. Komjathy, E. B. Shume, and M. Crespi (2021). GNSS total variometric approach: First demonstration of a tool for real-time tsunami genesis estimation, *Sci. Rep.* **11,** no. 1, 3114, doi: 10.1038/s41598-021-82532-6.

Ruhl, C. J., D. Melgar, A. I. Chung, R. Grapenthin, and R. M. Allen (2019). Quantifying the value of real-time geodetic constraints for earthquake early warning using a global seismic and geodetic data set, *J. Geophys. Res.* **124,** no. 4, 3819–3837, doi: 10.1029/2018jb016935.

Ruhl, C. J., D. Melgar, J. Geng, D. E. Goldberg, B. W. Crowell, R. M. Allen, Y. Bock, S. Barrientos, S. Riquelme, J. C. Baez, *et al.* (2018). A global database of strong-motion displacement GNSS recordings and an example application to PGD scaling, *Seismol. Res. Lett.* **90,** no. 1, 271–279, doi: 10.1785/0220180177.

Ruhl, C. J., D. Melgar, R. Grapenthin, and R. M. Allen (2017). The value of real-time GNSS to earthquake early warning, *Geophys. Res. Lett.* **44,** no. 16, 8311–8319, doi: 10.1002/2017gl074502.

Savastano, G., A. Komjathy, O. Verkhoglyadova, A. Mazzoni, M. Crespi, Y. Wei, and A. J. Mannucci (2017). Real-time detection of tsunami ionospheric disturbances with a stand-alone GNSS receiver: A preliminary feasibility demonstration, *Sci. Rep.* **7,** no. 1, 46607, doi: 10.1038/srep46607.

Taboada, A., L. A. Rivera, A. Fuenzalida, A. Cisternas, H. Philip, H. Bijwaard, J. Olaya, and C. Rivera (2000). Geodynamics of the northern Andes: Subductions and intracontinental deformation (Colombia), *Tectonics* **19,** no. 5, 787–813, doi: 10.1029/2000tc900004.

The pandas development team (2024). pandas-dev/pandas: Pandas, doi: 10.5281/zenodo.10957263.

Tian, D., L. Uieda, W. J. Leong, Y. Fröhlich, W. Schlitzer, M. Grund, M. Jones, L. Toney, J. Yao, Y. Magen, *et al.* (2024). PyGMT: A Python interface for the Generic Mapping Tools, doi: 10.5281/zenodo.11062720.

Trenkamp, R., J. N. Kellogg, and J. T. Freymueller (2002). Wide plate margin deformation, southern Central America and northwestern South America, CASA GPS observations, *J. South Am. Earth Sci.* **15,** no. 2, 157–171, doi: 10.1016/s0895-9811(02)00018-4.

Velandia, F., J. Acosta, R. Terraza, and H. Villegas (2005). The current tectonic motion of the northern Andes along the Algeciras fault system in SW Colombia, *Tectonophysics* **399,** nos. 1–4, 313–329, doi: 10.1016/j.tecto.2004.12.028.

Wessel, P., and J. F. Luis (2017). The GMT/MATLAB Toolbox, *Geochem. Geophys. Geosyst.* **18,** no. 2, 811–823, doi: 10.1002/2016gc006723.

Wu, Y.-M., and L. Zhao (2006). Magnitude estimation using the first three seconds *P*-wave amplitude in earthquake early warning, *Geophys. Res. Lett.* **33,** no. 16, 786–4, doi: 10.1029/2006gl026871.

Manuscript received 23 November 2023
Published online 9 August 2024